scientific reports

Check for updates

OPEN

Room-temperature $FeSi_2$-doped Cu_2Se thermoelectric films with enhanced figure of merit

Masahiro Goto[1]✉, Michiko Sasaki[1]✉, Taku Moronaga[2], Toru Hara[3] & Yibin Xu[4]

Thermoelectric (TE) materials offer a promising pathway toward achieving carbon neutrality by converting waste heat into electricity. The enhancement of their figure-of-merit (zT) depends on optimizing the composition of materials and nanostructures, reducing the thermal conductivity, and increasing the power factor. Cu_2Se, a superionic material, achieves a zT of 0.4 at 300 K by facilitating Cu ion movement within its face-centered cubic lattice, effectively suppressing thermal conductivity. Herein, we present a novel TE material developed by doping Cu_xSe crystals of different compositions with $FeSi_2$. We report a remarkable zT of 0.69 at 298 K for Cu_2Se-based materials and reveal the presence of the CuO and Cu_2O tiny crystals on the material surface, uniform dispersion of Si within the film, and formation of distinctive amorphous FeO. Our strategy holds great potential for notably advancing waste heat recovery in sustainable TE materials.

Keywords Thermoelectric, Cu_2Se, Sputter, Thin film, Composite, $FeSi_2$

Developing thermoelectric (TE) materials capable of efficiently converting waste heat into electricity is crucial for achieving energy goals aligned with carbon neutrality[1,2]. Since approximately 90% of the thermal energy is dissipated at temperatures below 600 K, TE materials with enhanced performance near room temperature are in high demand, especially as autonomous energy sources for wearable sensing devices[3]. The conversion efficiency from thermal to electric energy is characterized by the dimensionless figure-of-merit, $zT = S^2\sigma T/\kappa$, where S is the Seebeck coefficient, σ is the electrical conductivity, $S^2\sigma$ is the power factor (PF), T is the temperature, and κ is the thermal conductivity. Improving the TE conversion efficiency requires innovative strategies to reduce thermal conductivity and enhance the power factor through the optimization of the material type, composition, interfaces, and nanostructures. Despite considerable progress, the zT values for commercial TE materials, such as Bi_2Te_3 (n-type) and $Bi_{0.5}Sb_{1.5}Te_3$ (p-type), remain limited to ~0.7 at room temperature (300 K), corresponding to ~7% conversion efficiency, which is considerably smaller than ~20% efficiencies reported for commercial photovoltaic modules. In particular, there are few p-type thermoelectric materials that exhibit high zT values, and the development of novel p-type thermoelectric materials are expected. This large difference highlights the pressing need to improve the conversion efficiency of sustainable, cost-effective TE materials, which is crucial for their widespread adoption. Achieving this goal aligns with the primary objective of installing TE element modules over large areas for extended periods, satisfying performance and sustainability requirements.

Furthermore, thermal conductivity, Seebeck coefficient, and electrical conductivity are the main material properties that dictate the improvement of dimensionless zT. However, their intercorrelated effects hinder the enhancement of the TE performance. The use of phonon-glass electron-crystal (PGEC) materials are among the most popular solutions to address these challenges because they exhibit glass-like behavior for phonons, reducing thermal conductivity. Moreover, they exhibit crystalline behavior for electrons, thereby enhancing electrical conductivity, which can considerably improve zT[4].

Recent research efforts have focused on optimizing TE materials, including the optimization of the BiN[5] thermoelectric properties, prediction of high zT values for ternary transition-metal nitride halide monolayers, such as ZrNI or HfNI[6], through data science methods, and investigation of the 2D GeTe/arsenene van der

[1]Thermal Energy Materials Group, Research Center for Materials Nanoarchitectonics (MANA), National Institute for Materials Science (NIMS), 1-2-1 Sengen, Tsukuba, Ibaraki 305-0047, Japan. [2]Electron Microscopy Unit, Materials Fabrication and Analysis Platform, Research Network and Facility Services Division, National Institute for Materials Science (NIMS), 1-2-1 Sengen, Tsukuba, Ibaraki 305-0047, Japan. [3]Microstructure Analysis Group, Research Center for Structural Materials, National Institute for Materials Science (NIMS), 1-2-1 Sengen, Tsukuba, Ibaraki 305-0047, Japan. [4]Data-Driven Inorganic Materials Group, Center for Basic Research on Materials, National Institute for Materials Science (NIMS), 1-2-1 Sengen, Tsukuba, Ibaraki 305-0047, Japan. ✉email: goto.masahiro@nims.go.jp; sasaki.michiko@nims.go.jp

Waals heterostructure[7]. In addition, studies have explored cobalt-containing sintered silicon–germanium alloys[8] and p-type $Ta_{0.42}Nb_{0.3}V_{0.15}Ti_{0.13}FeSb$ thermoelectric materials and performed composition optimizations in the quaternary phase space of half-Heusler compounds[9]. Further enhancements in the spin-driven thermopower and zT value without compromising electrical conductivity have been achieved using temperature-driven spin crossover, as observed in 5% Cr-doped MnTe[10]. Additionally, an increase in the room-temperature thermoelectricity with tensile strain in $SrTiO_3$-based superlattices, such as $[(SrTiO_3)m/(SrTi_{0.8}Nb_{0.2}O_3)_n]_t$, on $DyScO_3(110)$ substrates has been achieved[11]. Furthermore, TE property enhancement has been observed in Bi_2Te_3 through combinatorial gradient annealing technique[12]. A significant breakthrough is the improvement in TE performance through quadruple-band synglisis, which promotes the convergence of the energies and momenta of four valence bands[13]. In particular, selenium (Se)-alloyed SnS materials using quadruple-band synglisis demonstrate a high zT of ~1.0 at 300 K[13], making them promising for advancement of room-temperature TE materials.

Cu_2Se is a well-known and attractive superionic conductive PGEC material in which Cu ions exhibit liquid-like behavior within a stable Se crystal lattice. Cu_2Se undergoes a phase transition from a monoclinic α-phase to a cubic β-phase at ~400 K and is expected to improve zT through the PGEC phenomenon. Although the stable α-phase is suitable for the fabrication of TE devices, the high-temperature β-phase improves the Cu_2Se ionic conductivity but complicates the device fabrication[14]. In 2012, Liu et al.[15] and Yu et al.[16] reported zT values of 0.2 and 0.4, respectively, for bulk Cu_2Se at 300 K. In 2016[17], Perez-Taborda et al. demonstrated a high zT of 0.45 at room temperature by precisely controlling the overstoichometric $Cu_{2.075}Se$ composition in a Cu_2Se film. Interestingly, some investigations have reported remarkable zT values exceeding 400 within specific temperature ranges, particularly during structural phase transitions[18]. However, these achievements remain largely impractical for widespread applications as they have not yet surpass the performance of Bi_2Te_3 (n-type) and $Bi_{0.5}Sb_{1.5}Te_3$ (p-type). Therefore, various doping techniques have been explored to enhance the TE efficiency of Cu_2Se, incorporating substances such as Ga[19], Fe[20,21], Ni[20], Mn[20], In[20], Zn[20], Sm[20], Te[22,23], K[24], Cl[25], TiO_2[26], SiC[27], W[28], Au[29], Ti[30], Ag[31], BiCuSeO + graphene[32], Sb[33], Sn[34], BN[35], In(super lattice)[36] and Sc, Y, and La (first-principles investigations)[37]. Among these dopants, K doping yielded the highest zT of 0.56 at room temperature[24]. However, further improvements driven by simpler fabrication processes, safe and less toxic materials, and higher performance remain strongly desired.

Herein, to discover p-type thermoelectric materials with high zT at room temperature, we propose a novel method to improve the zT of Cu_2Se-based materials by incorporating small amounts of $FeSi_2$. Our approach involves incorporating multiple Cu_xSe crystal structures with different compositions to enhance the Seebeck coefficient while maintaining low thermal conductivity through increased interface density. The proposed method defines a strategy for low-cost, high-performance TE that can replace Bi_2Te_3 at room temperature, offering a pathway for the development of highly efficient devices.

Results and discussion

We prepared $Cu_2Se_xFe_ySi_zO_t$ (CSSFO) films using a combinatorial sputter coating system (COSCOS; see Methods) and modified the coating parameters by adjusting the substrate temperature from 298 K to 773 K and the radiofrequency (RF) power from 60 to 120 W (Supplementary Fig. S1)[38,39]. Energy-dispersive X-ray (EDX) spectroscopy was used to analyze the elemental composition of the CSSFO films under various fabrication conditions (Table 1, Supplementary Fig. S2). For CSSFO samples prepared at 773 K, the Cu-to-Se ratio was approximately 2.4, and the elemental composition remained stable as the RF power increased from 60 to 120 W. Conversely, the films produced at 60 W and 298 K exhibited a Cu-to-Se ratio of approximately 1.9 with a marginal increase in Fe and O concentrations, indicating that the substrate temperature and RF power considerably influence the elemental composition and properties of the films.

Figure 1 shows the dependence of the CSSFO films' TE properties on the RF power and substrate temperature. Cu_2Se crystals undergo a transition from the monoclinic α-phase to the face-centered cubic β-phase below 400 K. The results show that the CSSFO samples fabricated at 773 K exhibit a similar phase transition, although the phase transition temperature (PTT) shifts to 350 K and increases to 370 K with increasing RF power during coating. Repeating measurements three times up to 573 K confirmed that the material is thermally stable (Supplementary Fig. S3). However, the CSSFO films prepared at 60 W and 298 K exhibited no observable phase change in the Seebeck coefficient. electrical conductivity and PF measurements indicated a phase transition during the second measurement cycle, with the PTT occurring at ~400 K, which is consistent with that of conventional Cu_2Se. The electrical conductivity shown in Fig. 1a exhibits a peak value of ~4 MS/m for films produced at 60 W and 298 K. The sample prepared at 60 W and 773 K exhibited a lower electrical conductivity of ~1.5 MS/m, whereas the films produced at 80–120 W and 773 K demonstrated electrical conductivity values of 2.0–2.7 MS/m, with

Sample	Thickness (μm)	Composition (at%)					Cu/Se ratio
		O	Si	Fe	Cu	Se	
60 W, 298 K	9.37	8.8	0.2	1.4	58.8	30.8	1.9
60 W, 773 K	13.10	4.9	0.4	0.5	67.9	26.3	2.6
80 W, 773 K	11.75	3.3	0.2	0.5	67.5	28.5	2.4
100 W, 773 K	13.00	3.5	0.3	0.4	67.0	28.8	2.3
120 W, 773 K	13.25	5.1	0.3	0.3	65.7	28.6	2.3

Table 1. Elementary concentration of $Cu_2Se_xSi_yFe_zO_t$ films prepared under different synthesis conditions.

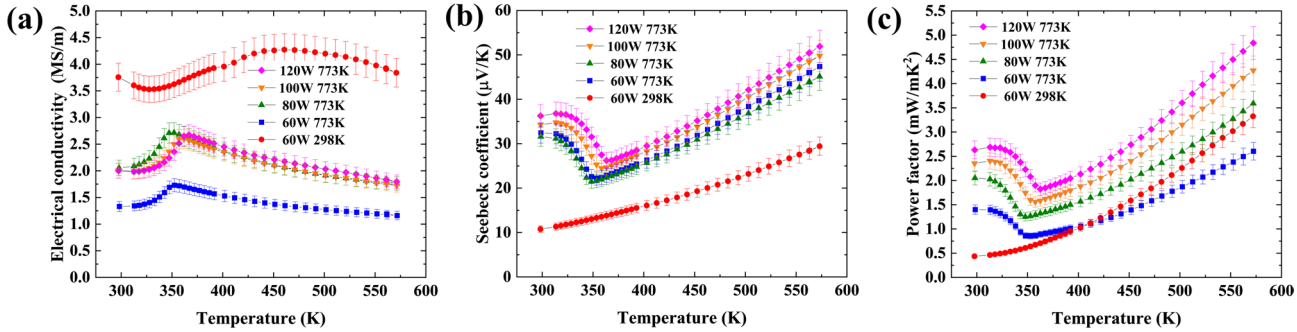

Fig. 1. Variation of the thermoelectric (TE) properties of $Cu_2Se_xSi_yFe_zO_t$ films with the radiofrequency (RF) power and substrate temperature. Temperature dependences of electrical conductivity (**a**), Seebeck coefficient (**b**), and power factor (**c**).

a maximum near the PTT. The electrical conductivity value for the 120-W sample at room temperature was twice as that of previously reported values[15], exhibiting excellent stability with temperature changes up to 573 K. The Seebeck coefficient shown in Fig. 1b varies from 20 to 38 μV/K in the α-phase (298–350 K) and from 20 to 53 μV/K in the β-phase for the 773 K samples. In contrast, the Seebeck coefficient for the 60 W and 298 K samples ranged from 10 to 30 μV/K, indicating no evidence of phase changes. The PF variation in the 298–573 K range is shown in Fig. 1c, ranging from 0.5 to 5.0 mW/mK^2. The samples prepared on the substrates at 773 K exhibit a consistent inflection point at PTT, which was absent in those prepared on the substrates at 298 K. At room temperature, the PF for CSSFO films reached 2.6 mW/mK^2, which is approximately 2.4 times greater than the previously reported value of 1.1 mW/mK^2[17]. This result represents the highest PF value reported for the Cu_2Se-based TEs, highlighting the potential of the CSSFO films for improved TE efficiency. Interestingly, among the 773 K samples, the Seebeck coefficient increases with RF power from 60 to 120 W, which suggests a decrease in carrier density. However, the electrical conductivity also increases across this range, remaining nearly constant between 80 and 120 W at 298 K. This simultaneous decrease in carrier density and increase in the electrical conductivity implies a substantial enhancement in carrier mobility. This effect is likely attributed to the promotion of microcrystallization and the influence of interfacial contributions—factors that will be discussed in detail later. Overall, these effects are strongly correlated with the dramatic improvement in PF.

Figure 2 shows the thermal conductivity and zT of the CSSFO films measured at room temperature. The thermal conductivity values range from 1.13 to 1.25 W/mK, which is slightly higher than that reported in the previous study (1.0 W/mK)[15]. The zT values exhibit considerable dependence on the RF power and substrate temperature. At 60 W, zT was measured at 0.11 and 0.35 for the substrate temperatures at 298 K and 773 K, respectively. For the samples on 773 K substrates, zT increased from 0.35 to 0.69 as the RF power increased from 60 to 120 W. Figure 3 compares the zT values of Cu_2Se-based materials in the literature depending on different types of doping. Liu et al.[15], Yu et al.[16], and Prez-Taborda et al.[17] reported zT values of 0.2–0.4 at room temperature for Cu_2Se without doping, which was recently reported at 0.45 by Ang et al. in 2023[31]. Although most doping attempts to exceed these zT values were unsuccessful, doping with K (zT = 0.56) and W (zT = 0.49) proved to be successful. In this study, we achieved a notable improvement in zT, reaching 0.69, approaching that of Bi_2Te_3 at room temperature, which is beneficial for TE applications due to its reduced cost and lower toxicity. The thermal conductivity of the Cu_2Se-based materials remains relatively stable across a broad temperature spectrum. Liu et al.[15] observed that thermal conductivity at 573 K is comparable to that at room temperature; thus, using our measured thermal conductivity value of 1.13 W/mK at room temperature, zT for the CSSFO samples at 573 K is estimated to be 2.45, which is remarkably high. The stoichiometric composition of Cu_2Se often yields a maximum zT of ~0.4[17]. Notably, the improvement in zT values achieved here strongly depends on the limitation of the RF power source of the sputter coating apparatus. Therefore, further research utilizing enhanced equipment and optimized fabrication configurations holds remarkable potential for achieving even higher zT values for CSSFO materials, offering low-cost, high-performance alternatives to Bi_2Te_3.

Figure 4 shows the scanning electron microscopy (SEM) and high-resolution transmission electron microscopy (HRTEM) micrographs of the CSSFO sample prepared at 120 W and 773 K (micrographs of the remaining samples are shown in Supplementary Fig. S4). Several fissures are visible on the thin film's surface in Fig. 4a. A close look at these fissures reveals clearly visible approximately 1–3-μm-sized crystal grains, as shown in the inset. When the surface is magnified, a tetrahedral-like structure is observed. A detailed observation using HRTEM reveals that the structure corresponds to a Cu_2O single crystal, as shown in Fig. 4b. High-resolution micrographs in Fig. 4c reveal that these micron-sized grains consist of a large number of fine crystals and interfaces, whereas the atomic-level observations in Fig. 4d show their polycrystalline orientations. X-ray diffraction (XRD) analysis was also carried out (Fig. 5 and Supplementary Fig. S5). The XRD and TE property data were analyzed using principal component analysis (PCA). The Lasso and random forest algorithms were used for analysis, yielding R^2 values of 0.90 and 0.60, respectively. Considering it higher accuracy, Lasso was selected for further analysis. The heatmap of the Lasso analysis results is shown in Supplementary Fig. S9. The zT contribution rates of various components were 90% for PC1 and 9% for PC2, respectively, accounting for nearly the entire variance. To improve the zT value, it is essential to reduce PC1 and PC2, which corresponds to weakening the 002 peak intensity of Cu_2Se at ~13°, while strengthening the 211 and 311 peak intensities

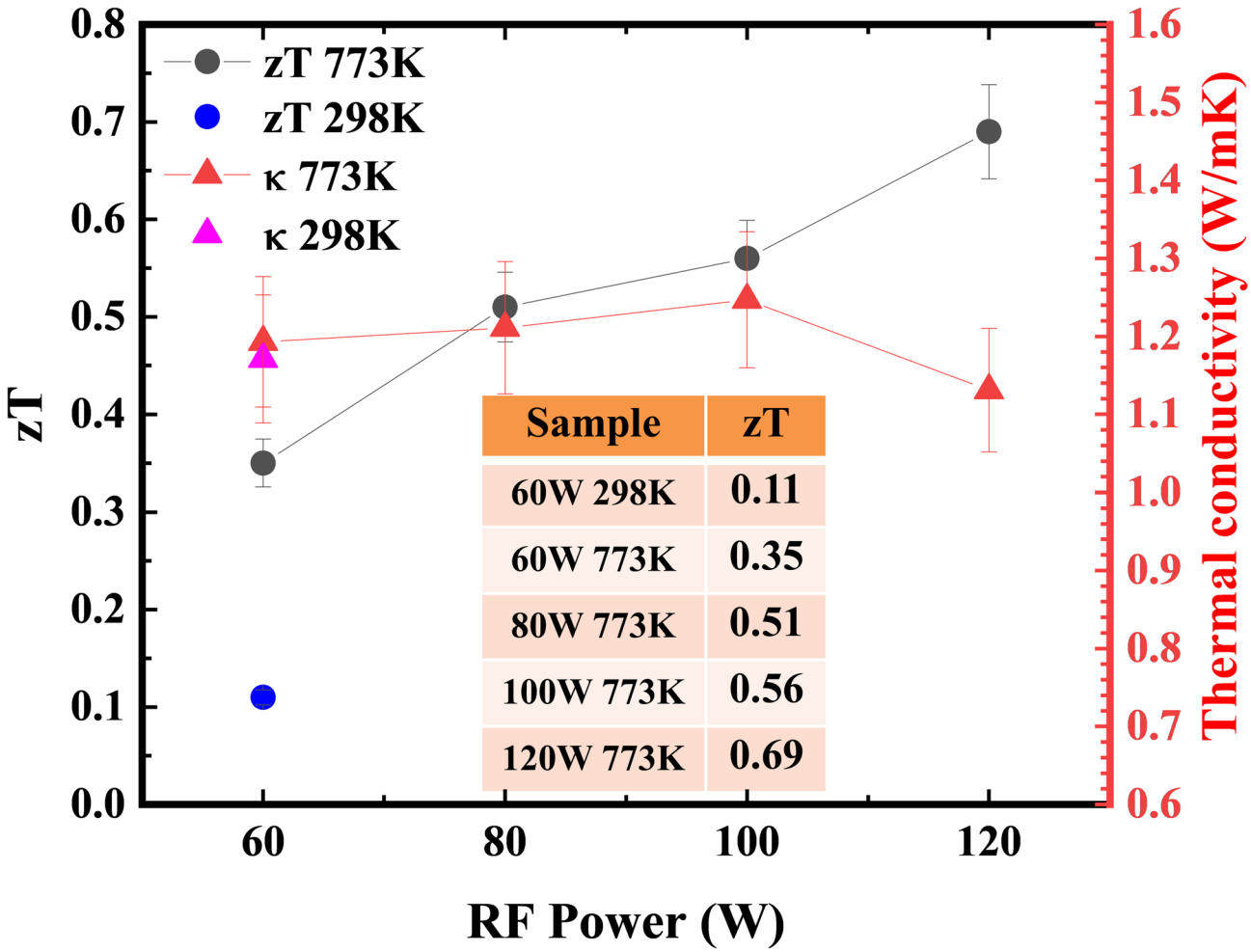

Fig. 2. Figure of merit (zT) and thermal conductivity (κ) of $Cu_2Se_xSi_yFe_zO_t$ thin films as a function of RF power and substrate temperature at room temperature (298 K).

observed at ~25.5° and 220 peak intensity at ~44°. In addition, increasing the peak intensities of $Cu_{1.82}Se$ and $Cu_{1.8}Se$ is beneficial. This suggests that the sufficient growths of the Cu_2Se, $Cu_{1.82}Se$, and $Cu_{1.8}Se$, tiny crystals are crucial for improving the TE performance of the material.

The XRD spectrum of the CSSFO sample at 120 W and a 773 K substrate shows several phases, including Cu_2Se, $Cu_{1.82}Se$, $Cu_{1.8}Se$, Cu_2O, and CuO. However, the CSSFO sample prepared at 298 K mainly comprised Cu_2Se crystals, while the CSSFO samples at 773 K were a mixture of $Cu_{1.82}Se$, $Cu_{1.8}Se$, and Cu_2Se tiny crystals. Additionally, as the RF power increased, the peak intensities of the $Cu_{1.82}Se$ and $Cu_{1.8}Se$ crystals increased, whereas the Cu_2Se peak decreased. No XRD peaks corresponding to Fe and Si were observed due to their metastable structures. Figure 6 shows the EDX elemental maps for the CSSFO sample at 120 W and 773 K. Si was uniformly distributed across the film, whereas Fe was detected in granular form within an amorphous iron oxide structure. Thus, the integration of a small quantity of $FeSi_2$ during the sputter coating process led to the formation of various complex crystal structures within the Cu_xSe matrix. These structural differences improved the Seebeck coefficient by creating multiple surfaces, which led to a decrease in thermal conductivity. Furthermore, the oxidation across the entire film led to the formation of Cu_2O and CuO on the surface, whereas FeO was evenly distributed within the film structure.

First-principles calculations are an effective method for analyzing the thermoelectric properties; however, the calculations of nonstoichiometric $Cu_{2-x}Se$ materials are difficult due to the existence of 3d electrons in Cu. Domashevskaya et al.[40] investigated the band structure and electron density of $Cu_{2-x}Se$ using X-ray photoelectron spectroscopy (XPS) and X-ray emission spectroscopy(XES). They showed that the magnitude of p-band splitting depended on the change in the value of x in $Cu_{2-x}Se$ and that the value of the band gap varied with the x value. This result indicates that present materials are a complex mixture of nanocrystals with three band gaps. TE efficiency in SnS crystals arises due to an increased convergence of the energy and momentum of four valance bands, termed as quadruple-band synglisis[13]. Furthermore, TE properties can be improved by actively introducing vacancies and activating multiple band synthesis. Our samples are composite materials with different band gaps of Cu_2Se, $Cu_{1.82}Se$, and $Cu_{1.8}Se$. While the interaction among these three band gaps may contribute to an enhancement in zT, isolating the underlying mechanisms proved difficult due to

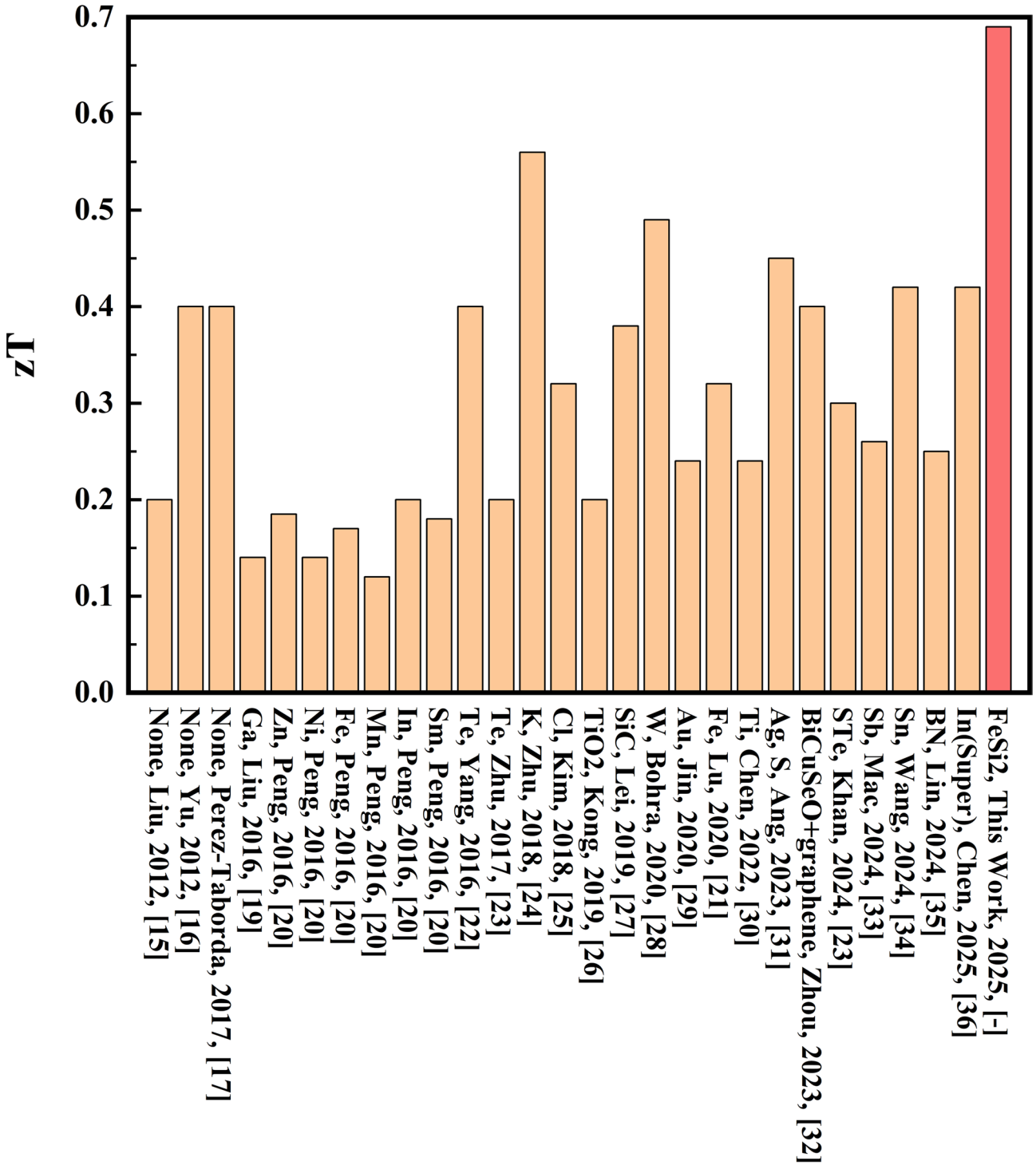

Fig. 3. Comparison of zT values at room temperature with previous studies and this work.

the concurrent effects of interfacial phenomena, interlayer stress, and electronic interactions between different phases. Importantly, the coexistence of multiple thermoelectric tiny crystals and the introduction of numerous interfaces contributed to the observed improvement in zT. These results demonstrate the importance of $FeSi_2$ doping in facilitating diverse crystal formations and optimizing TE properties through nanostructuring and interface engineering.

Methods

CSSFO samples were synthesized using COSCOS, which is a homemade sputter coating system, as shown in Supplementary Fig. S1. The samples were prepared on floating potential quartz substrates measuring $22 \times 4 \times 1.5$

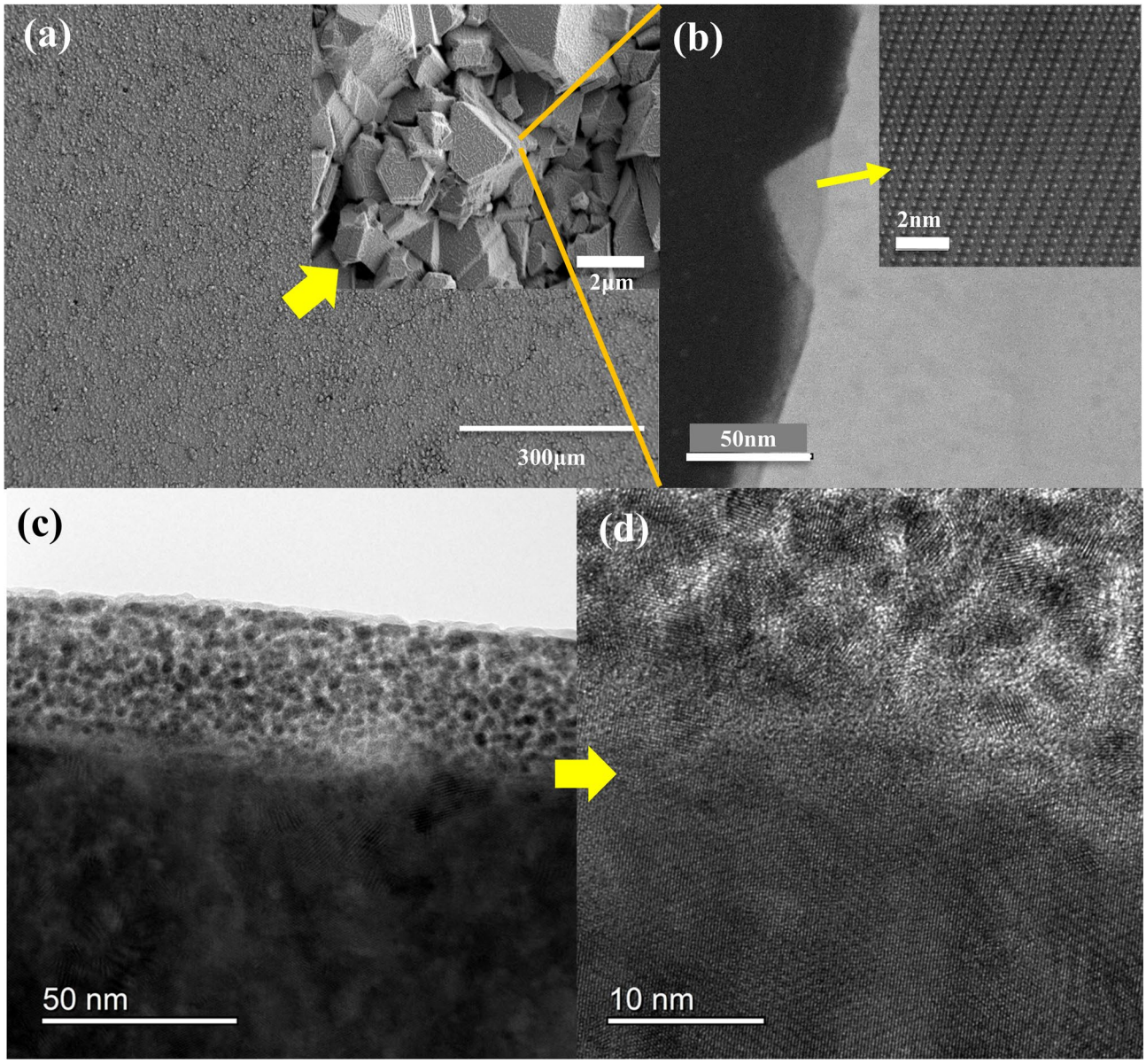

Fig. 4. Scanning electron microscopy (SEM) and high-resolution transmission electron microscopy (HRTEM) images of $Cu_2Se_{0.87}$ $Si_{0.01}Fe_{0.01}O_{0.16}$ thin films. SEM images of the $Cu_2Se_{0.87}Si_{0.01}Fe_{0.01}O_{0.16}$ films with radiofrequency (RF) power of 120 W and substrate temperature of 773 K (**a**). The thin film exhibits numerous cracks and micron-sized crystal grains grown on its surface. (inset). A tetrahedron-like structure is observed when zooming in on the crack areas. Detailed observation of the tetrahedron-like structure using HRTEM revealed that it was a single crystal of Cu_2O (**b**). Cross-sectional HRTEM image of the film (**c**). Multiple small crystals exist within the film in different orientations (**d**). The sample surface of panels (**c**) and (**d**) covered by a carbon protective film.

mm^3, supplied by Hiraoka Special Glass Mfg. Co. (Japan). Sputter coating was conducted with ultra-high purity argon gas (99.999%) and a Cu_2Se sputter target with a diameter and thickness of 50 and 4 mm, respectively. The operational argon gas pressure was maintained at 0.4 Pa. A 3-mm thick $FeSi_2$ sputter-coated shutter was used for $FeSi_2$ doping, with 5% of the coated area overlapping the target during the coating process to ensure precise doping. The introduction of $FeSi_2$ into the plasma facilitated the co-sputtering of Fe and Si atoms, allowing trace quantities to be incorporated into the films. The overlapped area was kept constant but could be modified to control the doping levels. The distance between the target and substrate was fixed at 55 mm. Pre-sputtering was performed for 15 min to ensure target stability, and a quartz crystal thickness monitor along with cross-sectional scanning transmission electron microscopy (STEM) measurement (9.37–13.25 μm) were used to ensure uniform thickness. During sputtering, the RF power was varied between 60 and 120 W, and the substrate temperature was adjusted from 298 K to 773 K, respectively. The surface morphology and elemental composition were examined using SEM (JEOL JSM-7900 F, FEI Electron Optics Thermo Scientific Scios2 HiVac, and Hitachi High-Tech

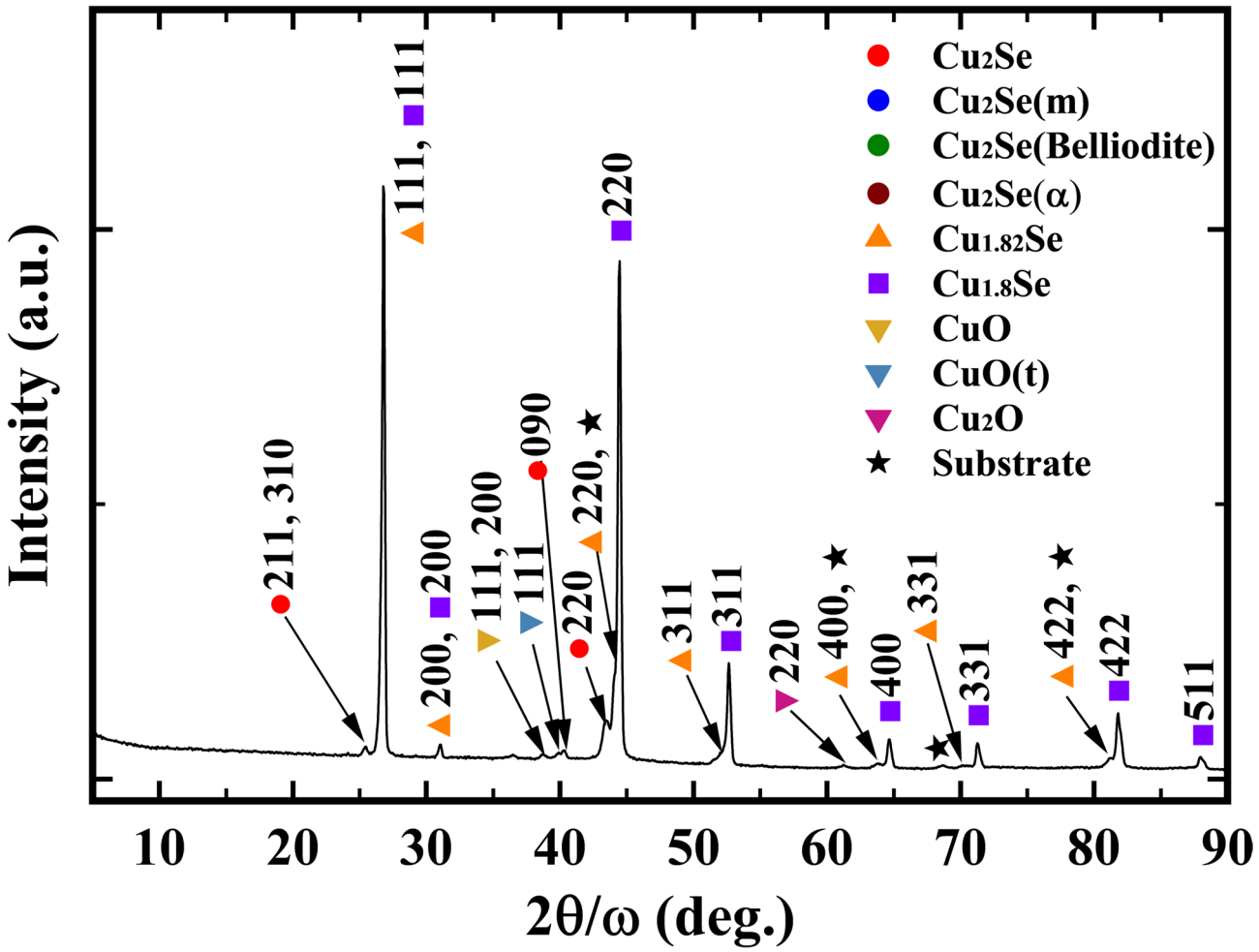

Fig. 5. X-ray diffraction (XRD) spectra of $Cu_2Se_{0.87}$ $Si_{0.01}Fe_{0.01}O_{0.16}$ thin film at 120 W and 773 K. Peaks corresponding to Cu_2Se, $Cu_{1.82}Se$, $Cu_{1.8}Se$, Cu_2O, and CuO crystals are observed. Peaks marked with a star are due to the substrate.

S-3700) and EDX (JEOL JED-2300 Analysis Station Plus), respectively. The Seebeck coefficient and electrical conductivity were measured using a Netzsch SBA 458 Nemesis® (Spain) system with the 4-point method and He gas for thermal insulation. Thermal conductivity (κ) was estimated using the formula $\kappa = TD \times Cp \times d$, where TD denotes the thermal diffusivity, Cp denotes the heat capacity, and d denotes the density. Thermal diffusivity was measured using ai-Phase type-1u at 298 K. The Cp and d values of 0.354 J/gK and 6.3 g/cm^3, respectively, were taken from the literature[41]. STEM and electron diffraction were performed using an atomic resolution electron microscope (JEOL JEM-ARM300F GRAND ARM, Japan). The crystal structure of the samples was determined using XRD (Rigaku SmartLab, Japan). The XRD peaks were assigned based on the material database system (AtomWork, NIMS), and PCA analysis was performed by the WAVEBASE system (Toyota Motor Corporation, Japan).

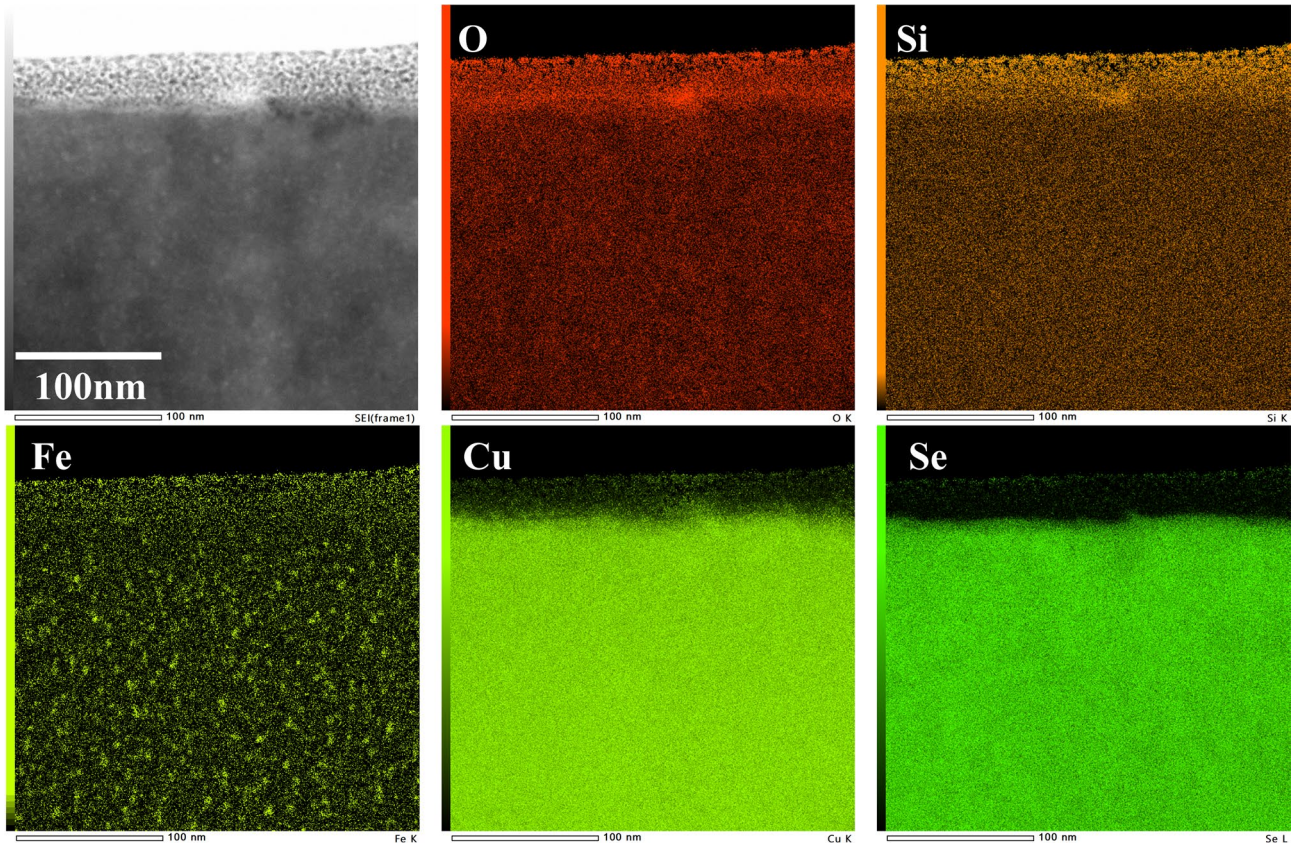

Fig. 6. Elemental maps of CSSFO films prepared at 120 W and 773 K using energy-dispersive X-ray spectroscopy.

Data availability

The authors declare that the data supporting the findings of this study are available within the paper, its supplementary information file.

Received: 21 March 2025; Accepted: 16 July 2025
Published online: 26 July 2025

References

1. Snyder, G. J. & Toberer, E. S. Complex thermoelectric materials. *Nat. Mater.* **7**, 105–114. https://doi.org/10.1038/nmat2090 (2008).
2. Mao, J., Chen, G. & Ren, Z. F. Thermoelectric cooling materials. *Nat. Mater.* **20**, 454–461. https://doi.org/10.1038/s41563-020-00852-w (2021).
3. Raj, A. & Steingart, D. Review-power sources for the internet of things. *J. Electrochem. Soc.* **165**, B3130–B3136. https://doi.org/10.1149/2.0181808jes (2018).
4. Wei, J. T. et al. Review of current high-ZT thermoelectric materials. *J. Mater. Sci.* **55**, 12642–12704. https://doi.org/10.1007/s10853-020-04949-0 (2020).
5. Remesal, E. R. et al. Enhancing the thermoelectric figure of merit of BiN polymorphism, pressure, and nanostructuring. *J. Mater. Chem. A*. **13**, 220–229. https://doi.org/10.1039/d4ta05891g (2024).
6. Anbarasan, R., Kim, D. & Park, J. H. Ternary transition-metal nitride halide monolayers MNI (M = Zr, Hf) with low thermal conductivity and high thermoelectric figure of merit. *Comp. Mater. Sci.* **247**, 113508. https://doi.org/10.1016/j.commatsci.2024.113508 (2025).
7. Balaji, A. S., Ramasamy, A., Sivasankar, K. J., Mohanraj, H. R. & Thiruvadigal, J. DFT + NEGF insights on boosting the thermoelectric figure of merit of 2D GeTe/arsenene vdW heterostructure device: Interface engineering. *Surf. Interfaces* **56**, 105534. https://doi.org/10.1016/j.surfin.2024.105534 (2025).
8. Grevtsov, N. et al. Thermoelectric materials based on cobalt-containing sintered silicon-germanium alloys. *Mater. Res. Bull.* **184**, 113258. https://doi.org/10.1016/j.materresbull.2024.113258 (2025).
9. Naderloo, R. H. et al. Performance advancements in P-type TaFeSb-based thermoelectric materials through composition and composite optimizations. *Energy Environ. Sci.* **18**, 738–749. https://doi.org/10.1039/d4ee04819a (2025).
10. Polash, M. M. H., Stone, M., Chi, S. X. & Vashaee, D. Designing spin-crossover systems to enhance thermopower and thermoelectric figure-of-merit in paramagnetic materials. *Energy Environ. Mater.* **8**, e12822. https://doi.org/10.1002/eem2.12822 (2025).
11. Zhu, Y. et al. Boosting room-temperature thermoelectricity in SrTiO-based superlattices. *J. Mater. Chem. C.* **13**, 2279–2285. https://doi.org/10.1039/d4tc04200j (2025).
12. Sasaki, M., Ju, S. H., Xu, Y. B., Shiomi, J. & Goto, M. Identifying optimal strain in bismuth telluride thermoelectric film by combinatorial gradient thermal annealing and machine learning. *ACS Comb. Sci.* **22**, 782–790. https://doi.org/10.1021/acscombsci.0c00112 (2020).

13. Liu, S. et al. Quadruple-band synglisis enables high thermoelectric efficiency in earth-abundant Tin sulfide crystals. *Science* **387**, 202–208. https://doi.org/10.1126/science.ado1133 (2025).
14. Brown, D. R., Day, T., Caillat, T. & Snyder, G. J. Chemical stability of $(Ag,Cu)_2Se$: A historical overview. *J. Electron. Mater.* **42**, 2014–2019. https://doi.org/10.1007/s11664-013-2506-2 (2013).
15. Liu, H. L. et al. Copper ion liquid-like thermoelectrics. *Nat. Mater.* **11**, 422–425. https://doi.org/10.1038/Nmat3273 (2012).
16. Yu, B. et al. Thermoelectric properties of copper Selenide with ordered selenium layer and disordered copper layer. *Nano Energy*. **1**, 472–478. https://doi.org/10.1016/j.nanoen.2012.02.010 (2012).
17. Perez-Taborda, J. A. et al. Pulsed hybrid reactive Magnetron sputtering for high Cu_2Se thermoelectric films. *Adv. Mater. Technol. -US*. **2**, 1700012. https://doi.org/10.1002/admt.201700012 (2017).
18. Byeon, D. et al. Discovery of colossal Seebeck effect in metallic Cu_2Se. *Nat. Commun.* **10**, 72. https://doi.org/10.1038/s41467-018-07877-5 (2019).
19. Liu, S. et al. Enhanced thermoelectric properties of β-Cu_2Se by incorporating CuGaSe. *J. Alloy Compd.* **688**, 521–526. https://doi.org/10.1016/j.jallcom.2016.07.218 (2016).
20. Peng, P. et al. Structure and thermoelectric performance of β-Cu_2Se doped with fe, ni, Mn. *Zn Or. Sm Intermetallics*. **75**, 72–78. https://doi.org/10.1016/j.intermet.2016.05.012 (2016).
21. Lu, R. M., Bailey, T. P., Uher, C. & Poudeu, P. F. P. Ultrafine interwoven dendritic Cu_2Se/CuFeSe composites with enhanced thermoelectric performance. *ACS Appl. Energy Mater.* **3**, 9133–9142. https://doi.org/10.1021/acsaem.0c01525 (2020).
22. Yang, L. et al. Te-doped Cu_2Se nanoplates with a high average thermoelectric figure of merit. *J. Mater. Chem. A*. **4**, 9213–9219. https://doi.org/10.1039/c6ta02998a (2016).
23. Zhu, Y. B., Zhang, B. P. & Liu, Y. Enhancing thermoelectric performance of Cu_2Se by doping Te. *Phys. Chem. Chem. Phys.* **19**, 27664–27669. https://doi.org/10.1039/c7cp05149b (2017).
24. Zhu, Z., Zhang, Y. W., Song, H. Z. & Li, X. J. Enhancement of thermoelectric performance of Cu_2Se by K doping. *Appl. Phys. A-Mater*. **124** https://doi.org/10.1007/s00339-018-2299-5 (2018).
25. Kim, M. J. et al. Effects of Cl-doping on thermoelectric transport properties of Cu_2Se prepared by spark plasma sintering. *J. Electron. Mater.* **48**, 1958–1964. https://doi.org/10.1007/s11664-018-6708-5 (2019).
26. Kong, F. F. et al. Ultralow thermal conductivity and high thermoelectric performance of Cu_2Se/TiO nanocomposite. *Appl. Phys. Lett.* **115**, 203901. https://doi.org/10.1063/1.5126152 (2019).
27. Lei, J. D. et al. High thermoelectric performance in Cu_2Se superionic conductor with enhanced liquid-like behaviour by dispersing SiC. *J. Mater. Chem. A*. **7**, 7006–7014. https://doi.org/10.1039/c8ta12210e (2019).
28. Bohra, A. K. et al. Stabilizing thermoelectric figure-of-merit of superionic conductor Cu_2Se through W nanoinclusions. *Phys. Status Solidi-R*. **14**, 2000102. https://doi.org/10.1002/pssr.202000102 (2020).
29. Jin, Y. et al. Size-controlled Au-Cu_2Se core-shell nanoparticles and their thermoelectric properties. *ACS Appl. Mater. Inter*. **12**, 36589–36599. https://doi.org/10.1021/acsami.0c08149 (2020).
30. Chen, Y. X., Zhang, Y. Y., Uher, C. & Poudeu, P. F. P. Carrier mobility modulation in Cu_2Se composites using coherent Cu_2TiSe inclusions leads to enhanced thermoelectric performance. *ACS Appl. Mater. Inter*. **14**, 56817–56826. https://doi.org/10.1021/acsami.2c17146 (2022).
31. Ang, A. K. R. et al. Development of Cu_2Se/Ag(S,Se)-Based monolithic thermoelectric generators for low-grade waste heat energy harvesting. *ACS Appl. Mater. Inter*. **15**, 46962–46970. https://doi.org/10.1021/acsami.3c09823 (2023).
32. Zhou, Z. F. et al. Compositing effects for high thermoelectric performance of Cu_2Se-based materials. *Nat. Commun.* **14**, 2410. https://doi.org/10.1038/s41467-023-38054-y (2023).
33. Mac, T. K. et al. Synthesis and thermoelectric characterization of Sb-doped Cu_2Se by mechanical alloying and solid-state reaction. *J. Electron. Mater.* **53**, 1026–1034. https://doi.org/10.1007/s11664-023-10808-w (2024).
34. Wang, Q. et al. Enhanced thermoelectric performance of Cu_2Se thin film derived from potential barrier scattering by incorporating SnSe nano-dispersions. *Appl. Phys. Lett.* **124**, 192104. https://doi.org/10.1063/5.0201400 (2024).
35. Lin, Z. H. et al. Impact of Boron nitride on the thermoelectric properties and service stability of Cu_2Se. *ACS Appl. Mater. Inter*. **17**, 1922–1930. https://doi.org/10.1021/acsami.4c16857 (2024).
36. Chen, Y., Song, G. H., Ben, Z. H., Wu, Y. S. & You, J. H. Improved thermoelectric properties of the β-Cu_2Se/CuInSe multilayer films by layer interface scattering. *Curr. Appl. Phys.* **70**, 1–10. https://doi.org/10.1016/j.cap.2024.11.010 (2025).
37. Benaadad, M., Nafidi, A., Melkoud, S., Khan, M. S. & Soubane, D. First-principles investigations of structural, optoelectronic and thermoelectric properties of Cu-based chalcogenides compounds. *J. Mater. Sci.* **56**, 15882–15897. https://doi.org/10.1007/s10853-021-06325-y (2021).
38. Goto, M., Kasahara, A. & Tosa, M. Low frictional property of copper oxide thin films optimised using a combinatorial sputter coating system. *Appl. Surf. Sci.* **252**, 2482–2487. https://doi.org/10.1016/j.apsusc.2005.03.236 (2006).
39. Goto, M. et al. Control of p-type and n-type thermoelectric properties of bismuth telluride thin films by combinatorial sputter coating technology. *Appl. Surf. Sci.* **407**, 405–411. https://doi.org/10.1016/j.apsusc.2017.02.187 (2017).
40. Domashevskaya, E. P. et al. XPS and XES emission investigations of d-p resonance in some copper chalcogenides. *J. Electron. Spectrosc.* **114**, 901–908. https://doi.org/10.1016/S0368-2048(00)00406-0 (2001).
41. Brown, D. R. et al. Relating phase transition heat capacity to thermal conductivity and effusivity in Cu_2Se. *Phys. Status Solidi-R*. **10**, 618–621. https://doi.org/10.1002/pssr.201600160 (2016).

Acknowledgements

This research was supported by Japan Science and Technology Agency (JST) CREST under the projects "Exploring Innovative Materials in Unknown Search Space" (JPMJCR21O2), CREST and "Scientific Innovation for Energy Harvesting Technology" (JPMJCR16Q5). A part of this work was also supported by Grant-in-Aid for Scientific Research (C) 24K07349 and 25K08337 from the Japan Society for the Promotion of Science (JSPS). A part of this work was supported by the Electron Microscopy Unit, National Institute for Materials Science (NIMS). We would like to thank Toyota Motor Corporation for allowing us to use the material analysis cloud service "WAVEBASE".

Author contributions

M.G. planned and supervised the study. M.S. and M.G. prepared the samples, characterized them using XRD and X-ray photoelectron spectroscopy, and measured their thermoelectric properties. M.G. and Y.X. performed thermal conductivity measurements. SEM, STEM, and EDX measurements were performed by T.M. and T.H. All authors discussed the results, developed explanations for experiments, and provided feedback on the manuscript. M.G. and M.S. wrote and edited the manuscript.

Declarations

Competing interests
The authors declare no competing interests.

Additional information
Supplementary Information The online version contains supplementary material available at https://doi.org/10.1038/s41598-025-12345-4.

Correspondence and requests for materials should be addressed to M.G. or M.S.

Reprints and permissions information is available at www.nature.com/reprints.

Publisher's note Springer Nature remains neutral with regard to jurisdictional claims in published maps and institutional affiliations.